Propagation of ULF waves through the ionosphere: Inductive effect for oblique magnetic fields

M. D. Sciffer, C. L. Waters, F. W. Menk

Annales Geophysicae (2004) 22: 1155–1169
SRef-ID: 1432-0576/ag/2004-22-1155

Annales Geophysicae

Propagation of ULF waves through the ionosphere: Inductive effect for oblique magnetic fields

M. D. Sciffer, C. L. Waters, and F. W. Menk

School of Mathematical and Physical Sciences and CRC for Satellite Systems
The University of Newcastle, Callaghan, 2308
New South Wales, Australia

Received: 29 April 2003 – Revised: 20 October 2003 – Accepted: 20 November 2003 – Published: 2 April 2004

Abstract. Solutions for ultra-low frequency (ULF) wave fields in the frequency range 1–100 mHz that interact with the Earth's ionosphere in the presence of oblique background magnetic fields are described. Analytic expressions for the electric and magnetic wave fields in the magnetosphere, ionosphere and atmosphere are derived within the context of an inductive ionosphere. The inductive shielding effect (ISE) arises from the generation of an "inductive" rotational current by the induced part of the divergent electric field in the ionosphere which reduces the wave amplitude detected on the ground. The inductive response of the ionosphere is described by Faraday's law and the ISE depends on the horizontal scale size of the ULF disturbance, its frequency and the ionosphere conductivities. The ISE for ULF waves in a vertical background magnetic field is limited in application to high latitudes. In this paper we examine the ISE within the context of oblique background magnetic fields, extending studies of an inductive ionosphere and the associated shielding of ULF waves to lower latitudes. It is found that the dip angle of the background magnetic field has a significant effect on signals detected at the ground. For incident shear Alfvén mode waves and oblique background magnetic fields, the horizontal component of the field-aligned current contributes to the signal detected at the ground. At low latitudes, the ISE is larger at smaller conductivity values compared with high latitudes.

Key words. Ionosphere (ionosphere-magnetosphere interactions; electric fields and currents; wave propagation)

1 Introduction

Ultra-low frequency (ULF) waves in the 1–100 mHz band are generated by processes involving the interaction of the solar wind with the Earth's magnetosphere. These ULF perturbations propagate towards the ionosphere where they are partially reflected and may be detected using ground-based magnetometers. The cold magnetospheric plasma supports the fast and shear Alfvén magnetohydrodynamic (MHD) wave modes (e.g. Stix, 1962; Alfvén and Falthammar, 1963). The interaction of ULF waves with the ionosphere creates current systems that modify the amplitude and spatial scale size of the waves as deduced from ground-based magnetometer arrays (Nishida, 1964; Hughes and Southwood, 1976). In order to construct a coherent view of ULF signals measured by ground-based magnetometers, radars and satellites, the effect of the ionosphere and associated current systems needs to be understood.

The ionosphere presents a conducting interface between the magnetosphere and atmosphere. While the altitude of the ionosphere is much smaller than typical ULF wavelengths, the anisotropic conductivity of the ionosphere and currents generated by the waves give complicated ground level wave field solutions (Hughes, 1974; Hughes and Southwood, 1976; Ellis and Southwood, 1983; Yoshikawa and Itonaga, 1996; 2000). One well-known effect of the ionosphere on ULF wave properties is a 90° rotation of the wave magnetic field, $\boldsymbol{b}$, when comparing the signal in the magnetosphere with the signal at the ground. For a horizontally uniform ionosphere, the 90° rotation is a direct result of the field-aligned current associated with a shear Alfvén mode wave meeting the neutral atmosphere, where $\nabla \times \boldsymbol{b}=0$ (Hughes, 1983). This was described as a "shielding" of the magnetospheric wave field component from the ground that may be seen as a rotation of the wave polarisation azimuth with altitude.

An inductive shielding effect (ISE) was discussed by Yoshikawa and Itonaga (1996) for the case where the Earth's background magnetic field, ($\boldsymbol{B_0}$), is vertical. The ISE may be understood in terms of the properties of the wave electric field, $\boldsymbol{e}$. If $\nabla \times \boldsymbol{e}$ is significant, then Faraday's inductive term may cause a reduction in the amplitude of the wave seen on the ground, compared with that in the magnetosphere (Yoshikawa and Itonaga, 1996; 2000). Early studies of the interaction of ULF waves with the ionosphere were

Correspondence to: C. L. Waters
(colin.waters@newcastle.edu.au)

formulated for low frequency (1–5 mHz) ULF waves and for spatial scale sizes that resulted in a negligible ISE (e.g. Nishida, 1964). At middle to low latitudes, the shear Alfvén wave mode can form field line resonances (e.g. Miletits et al., 1990; Waters et al., 1991; Ziesolleck et al., 1993), so that the resonant frequency increases into the Pc3 (20–100 mHz) range with decreasing latitude. A formulation which includes inductive effects and allows for oblique $\boldsymbol{B_0}$ is necessary for describing the interaction of ULF waves with the ionsophere at these latitudes.

The interaction of ULF waves with the ionosphere in the presence of an oblique $\boldsymbol{B_0}$ was discussed by Tamao (1986), who pointed out two approaches to the problem. In the high latitude ionosphere, particularly around the auroral zones, field-aligned currents (FACs) may be associated with Alfvén waves and particle precipitation. For regions where the dominant energy mechanism is via the particles, a FAC description is appropriate. For mid to low latitudes a formulation based on the wave fields is more suitable. For vertical $\boldsymbol{B_0}$ and uniform ionosphere, Tamao (1964) showed that the ground magnetic variations were only due to induced ionosphere Hall currents. For oblique $\boldsymbol{B_0}$, Tamao (1986) showed the ground magnetic signal depends on both the Pedersen and Hall conductivities plus a direct contribution from FACs, depending on the spatial scale size of the disturbance. However, the ISE was not discussed and the model did not include a boundary at the ground.

The majority of published analytic solutions that describe the interaction of ULF waves with the ionosphere have assumed that $\boldsymbol{B_0}$ is either horizontal (Zhang and Cole, 1995) or vertical (Nishida, 1964; Hughes, 1974; Hughes and Southwood, 1976). The problem may be further simplified by assuming $\nabla\times\boldsymbol{e}\rightarrow 0$, where Scholer (1970) showed that the reflection coefficient for a shear Alfvén mode wave incident on the ionosphere is given by

$$\Gamma_{11}^{\text{static}} = \frac{\Sigma_a - \Sigma_P}{\Sigma_a + \Sigma_P} = \frac{1-\alpha_P}{1+\alpha_P}, \tag{1}$$

where $\Sigma_a = \frac{1}{\mu_0 V_a}$ is the Alfvén wave conductance, Σ_P is the height integrated Pedersen conductivity and $\alpha_P = \frac{\Sigma_P}{\Sigma_a}$. While Tamao (1986) and Allan and Poulter (1992) discussed the passage of a fast mode wave through the ionosphere, most studies have focused on the shear Alfvén mode, since typical model parameters for high latitudes give rise to an evanescent fast mode. At lower latitudes, the fast mode may no longer be evanescent (e.g. Waters et al., 2001) and the full reflection coefficient and mode conversion matrix, including an oblique $\boldsymbol{B_0}$, needs to be considered (Sciffer and Waters, 2002).

The ionosphere/atmosphere system influences ULF waves so that wave amplitudes in the magnetosphere are not necessarily equal to the amplitudes measured at the ground. "Shielding of the wave" is a common expression that describes the reduction of the ULF wave amplitude. However, there are a number of mechanisms that can "shield" ULF waves within the context of the magnetosphere/ionosphere/atmosphere/ground system. These are (i) the atmospheric shielding effect (ASE) (Hughes, 1974; Nishida, 1964, 1978), (ii) the inductive shielding effect (ISE) (Yoshikawa and Itonaga, 1996), and (iii) a 90° rotation of the wave fields (NDR) (Hughes, 1974, 1983; Hughes and Southwood, 1976). Hughes (1974) and Nishida (1978) showed that for high latitudes (vertical $\boldsymbol{B_0}$), a horizontally uniform anisotropic ionosphere alters the amplitude of ULF waves at the ground compared to the incident field from the magnetosphere according to

$$\delta b_\perp = 2\frac{\Sigma_H}{\Sigma_P}\exp(-|k_\perp|d)\delta b_A^{\text{i}}, \tag{2}$$

where δb_A^{i} is the incident magnetic field of the shear Alfvén wave which is associated with a FAC, d is the height between the ground and the ionospheric current sheet, $k_\perp$ is the horizontal wave number, and Σ_H is the height integrated Hall conductivity. The analytic formulation in Eq. (2) was developed assuming small frequencies and horizontal scale sizes (large $|k_\perp|$) and small Hall conductivity. These assumptions imply $\Sigma_P \gg \Sigma_H$, which reduces the effect of the rotational current system in the ionosphere (Yoshikawa and Itonaga, 1996). This essentially assumes an electrostatic ionosphere (Miura et al., 1982).

Both the ASE and NDR effects are evident in Eq. (2). For evanescent wave solutions in the vertical direction in the atmosphere, (i.e. $|k_\perp| \gg |\frac{\omega}{c}|$), the $\exp(-|k_\perp|d)$ term in Eq. (2) describes how localised wave fields decrease in amplitude with altitude in the neutral atmosphere to the ground. The NDR effect for an incident shear Alfvén wave was discussed and illustrated by Hughes (1974, 1983). For completeness and for further reference, a brief description is repeated here. Assume a vertical $\boldsymbol{B_0}$ and an incident shear Alfvén mode which has the wave magnetic field, $\boldsymbol{b}$, in the $\boldsymbol{y}$ direction. This places both $k_\perp$ and the incident wave electric field, $\boldsymbol{e}$, in the $\boldsymbol{x}$ direction (see Fig. 1 for the coordinate system used). In the magnetosphere, $(\nabla\times\boldsymbol{b})_\parallel = \mu_0 j_\parallel$, while for the atmosphere, $\nabla\times\boldsymbol{b}=0$. Therefore, $\boldsymbol{b}$ is either zero or in the direction of $k_\perp$ in the atmosphere. Even if the fast mode is evanescent in the magnetosphere, some fast mode signal can appear in the topside ionosphere due to finite Hall conductivity and the resulting wave mode conversion. The 90° rotation in the wave polarisation azimuth may require tens or more kilometers, depending on the evanescent properties of the fast mode wave. This feature is discussed further in Sect. 4. For a thin sheet ionosphere, the change in wave polarisation azimuth from just above the ionosphere to the atmosphere is controlled by the ratio of poloidal (divergent) to toroidal (rotational) current systems in the ionosphere (Yoshikawa and Itonaga, 1996). It is this term which governs the proportion of toroidal current generated from the time varying poloidal current system. These Hall currents are the source of the magnetic field, $\delta b_\perp^{(\text{static})}$, measured at the ground. They generate perturbation magnetic fields in a direction perpendicular to the incident Alfvén wave magnetic field. If $\Sigma_H \rightarrow 0$, then there will be no perturbation at the ground, since there

is no conversion of toroidal to poloidal magnetic field in the ionosphere.

The ISE for a vertical $\boldsymbol{B_0}$ was discussed by Yoshikawa and Itonaga (1996, 2000) and Yoshikawa et al. (2002). These authors developed an expression for the ground magnetic field as

$$\delta b_\perp = 2\frac{\Sigma_H}{\Sigma_a+\Sigma_P}\exp(-|k_\perp|d)\times \left(b_A^{\mathrm{i}}(t) - \int_t^0 \exp(-\gamma\tau)\frac{\partial}{\partial\tau}b_A^{\mathrm{i}}(t-\tau)d\tau\right). \quad (3)$$

For $\alpha_P=\frac{\Sigma_P}{\Sigma_a}\gg 1$, the first term on the right-hand side of Eq. (3) is equivalent to Eq. (2). The second term of Eq. (3) represents the inductive response in the ionosphere, where γ represents the damping of the inductive response of the rotational current system. The time scale, γ^{-1}, becomes an indicator of the inductive effect, which is large for small $k_\perp$, large $\alpha_P=\frac{\Sigma_P}{\Sigma_a}$ and large $\alpha_H=\frac{\Sigma_H}{\Sigma_P}$. Yoshikawa et al. (2002) showed that for a vertical $\boldsymbol{B_0}$, the inductive response of the ionosphere shielded the ground magnetic wave fields for frequencies $\sim$ 20–100 mHz and a highly conducting ionosphere.

In this paper we develop analytic solutions for the interaction of ULF waves with an inductive ionosphere suitable for mid to low latitudes, where $\boldsymbol{B_0}$ is oblique and the frequencies may reach 100 mHz. For these conditions, the full wave reflection and mode conversion matrix, developed in Sciffer and Waters (2002), is included. The restriction that the wave in the atmosphere is evanescent in the vertical direction is retained. These general solutions for ULF wave interaction with the ionosphere show that the magnetic field dip angle has a significant effect on the inductive shielding effect for a highly conducting ionosphere. The consequences for the amplitude of ULF waves observed by ground magnetometers at middle and low latitudes are also discussed.

2 ULF wave model

Analytic solutions for the reflection and wave mode conversion coefficients for ULF waves interacting with the ionosphere/atmosphere/ground system for oblique $\boldsymbol{B_0}$ are described in Sciffer and Waters (2002). For continuity, the main equations from that paper are summarised and we then show how the wave electric and magnetic fields can be calculated, given details of the incident wave, such as amplitude, spatial structure, wave mode mix and polarisation properties. These expressions will be used to investigate the ISE for middle to low latitudes, where the ionosphere is immersed in an oblique $\boldsymbol{B_0}$.

The ionosphere is approximated as a thin, anisotropic conducting sheet in the XY plane at z=0, as shown in Fig. 1. The electrical properties of the ionosphere are described by height integrated Pedersen (Σ_P), Hall (Σ_H) and parallel or direct (Σ_d) conductivities. The magnetosphere is described by ideal MHD, where the field-aligned electric field is zero. In the atmosphere the current density, j^{atm}=0, while the ground is located at z=$-d$ and modeled as a perfect conductor. Two MHD wave modes exist in the cold plasma of the magnetosphere. The fast (or compressional) mode is isotropic in nature and the shear Alfvén (or torsional) mode has energy that propagates along the background magnetic field (Priest, 1982; Cross, 1988). The wave in the neutral atmosphere is described by the solution to the linearized Faraday and Ampere laws and is evanescent in the vertical direction. Given that analytic solutions are known for the wave fields in both the magnetosphere and atmosphere, the problem is to match these solutions across the ionospheric current sheet using appropriate boundary conditions.

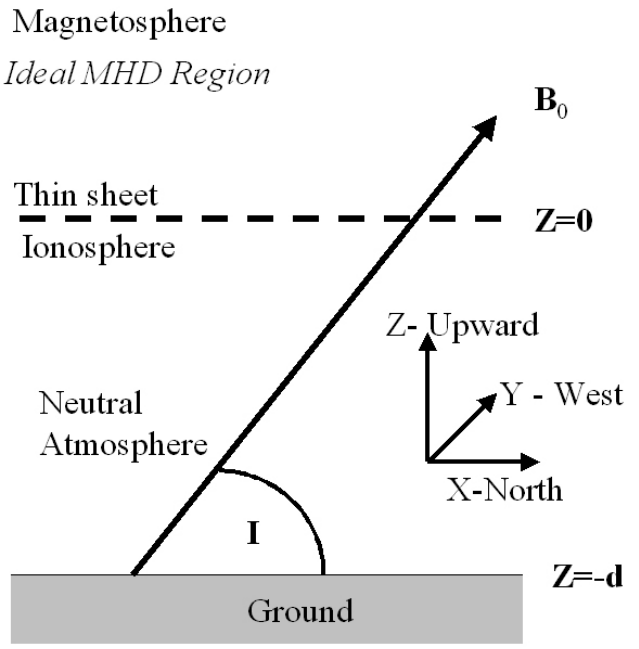

Fig. 1. Geometry of the magnetosphere, ionosphere and atmosphere used for the ULF wave propagation model.

The formulation is based on the boundary condition for the wave magnetic field, $\boldsymbol{b}$. The discontinuity in the magnetic field across the ionospheric current sheet is described by

$$(0,0,1)\times\left(\Delta b_x,\Delta b_y,0\right)=\mu_0\left(j_x,j_y,0\right), \quad (4)$$

where $(j_x, j_y, 0)$ is the current density in the sheet ionosphere and Δb_x and Δb_y represent the discontinuity in the wave magnetic fields.

The background magnetic field, $\boldsymbol{B_0}$, is confined to the XZ plane so that

$$\boldsymbol{B_0} = B_0\left[\cos(I),0,\sin(I)\right]. \quad (5)$$

The range and orientation of the dip angle, I, are choosen so that $0^\circ < I \leq 90^\circ$ for the Southern Hemisphere and $-90^\circ \leq I < 0^\circ$ for the Northern Hemisphere. The current density and electric fields in the ionosphere are related to the height integrated conductivity tensor, $\bar{\Sigma}$ in the usual way as

$$\boldsymbol{j}^I = \bar{\Sigma}\boldsymbol{e}^I. \quad (6)$$

The first order perturbation electric fields arising from ULF wave energy in the ionosphere are e_x^I, e_y^I and e_z^I. Assuming a temporal dependence of $e^{-j\omega t}$, Faraday's law is

$$j\omega \boldsymbol{b} = \nabla \times \boldsymbol{e}. \tag{7}$$

The contribution from $j\omega\boldsymbol{b}$ to the solution depends on the frequency of the waves. For Pc5 (1–5 mHz) waves the effect is quite small and can be neglected. However, for higher frequencies (20–100 mHz) often observed at middle and low latitudes $j\omega\boldsymbol{b}$ can be significant.

For ideal MHD conditions, electric fields are perpendicular to $\boldsymbol{B_0}$ (i.e. $e_\parallel$=0). Assuming an $e^{j(k_x x+k_y y)}$ horizontal wave structure, the two cold plasma ideal MHD wave modes may be identified by the relationship between their electric fields and wave numbers. The fast (or compressional) mode has

$$\nabla \cdot \boldsymbol{e} = 0 \qquad (\nabla \times \boldsymbol{e})_\parallel \neq 0. \tag{8}$$

From the fast mode dispersion relation, the vertical wave number is

$$k_{z,f} = \pm\sqrt{\frac{\omega^2}{V_a^2} - k_x^2 - k_y^2}, \tag{9}$$

where V_a is the Alfvén speed. From Eqs. (8) and (9), the electric field for the fast mode is proportional to a vector

$$\boldsymbol{P}_f = \left[P_{x,f},\, P_{y,f},\, P_{z,f}\right], \tag{10}$$

where $P_{x,f}$=$-k_y \sin(I)$, $P_{y,f}$=$k_x \sin(I)$−$k_{z,f}\cos(I)$ and $P_{z,f}$=$k_y \cos(I)$.

In particular, the electric field for the fast mode is expressed in terms of the $\boldsymbol{P}_f$ unit vector, $\hat{\boldsymbol{P}}_f$ as

$$\mathbf{e}_f = \beta\left[P_{x,f},\, P_{y,f},\, P_{z,f}\right]/|\mathbf{P}_f| = \beta\,\hat{\mathbf{P}}_f, \tag{11}$$

where β is a complex constant to be determined later.

For the shear Alfvén mode,

$$\nabla \cdot \boldsymbol{e} \neq 0 \qquad (\nabla \times \boldsymbol{e})_\parallel = 0. \tag{12}$$

From the dispersion relation, considering an oblique $\boldsymbol{B_0}$, the vertical wave number is

$$k_{z,a} = \frac{\pm\frac{\omega}{V_a} - k_x\cos(I)}{\sin(I)}. \tag{13}$$

From Eqs. (12) and (13) the electric field associated with the shear Alfvén mode is

$$\mathbf{e}_a = \alpha\left[P_{x,a},\, P_{y,a},\, P_{z,a}\right]/|\boldsymbol{P}_f| = \alpha\,\hat{\mathbf{P}}_a, \tag{14}$$

where α is a complex constant, $P_{x,a}$=$[k_x \sin(I)-k_{z,a}\cos(I)]\sin(I)$, $P_{y,a}$=k_y and $P_{z,a}$=$-[k_x \sin(I)-k_{z,a}\cos(I)]\cos(I)$. The total electric field in the magnetosphere is a superposition of the incident and reflected waves. From Eqs. (11) and (14) the total electric field components are

$$\begin{bmatrix} e_x^m(0) \\ e_y^m(0) \\ e_z^m(0) \end{bmatrix} = \alpha^r\,\hat{\boldsymbol{P}}_a^r + \alpha^i\,\hat{\boldsymbol{P}}_a^i + \beta^r\,\hat{\boldsymbol{P}}_f^r + \beta^i\,\hat{\boldsymbol{P}}_f^i, \tag{15}$$

where a denotes the shear Alfvén mode, f identifies the fast mode, and i and r represent incident and reflected waves, respectively. Therefore, $\hat{\boldsymbol{P}}_m^d$ (for d=i or r and m=a or f) is the unit vector in the direction of the electric field of the appropriate MHD wave mode. The α and β are amplitude factors from Eqs. (11) and (14). This superposition of the magnetospheric electric field allows for the wave fields and their derivatives to be expressed in terms of the composition of MHD wave modes present in the magnetosphere. The polarization of each wave mode is contained in the $\hat{\boldsymbol{P}}_m^d$.

In the atmosphere, the vertical wave number is

$$k_z^{\mathrm{atm}} = \sqrt{\frac{\omega^2}{c^2} - k_x^2 - k_y^2}. \tag{16}$$

A boundary condition at the ionosphere/atmosphere interface, ($z = 0$), specifies continuity of the horizontal electric fields. If the ground is a perfect conductor, then $e_x(-d)$=$e_y(-d)$=0. The solution in the atmosphere, ($-d \le z < 0$), is given by

$$e_x^{\mathrm{atm}} = e_x^m(0)\frac{\sinh[jk_z^{\mathrm{atm}}(z+d)]}{\sinh[jk_z^{\mathrm{atm}}(d)]}e^{j(k_x x+k_y y)} \tag{17}$$

$$e_y^{\mathrm{atm}} = e_y^m(0)\frac{\sinh[jk_z^{\mathrm{atm}}(z+d)]}{\sinh[jk_z^{\mathrm{atm}}(d)]}e^{j(k_x x+k_y y)} \tag{18}$$

$$e_z^{\mathrm{atm}} = \left(\frac{-k_x e_x^m(0) - k_y e_y^m(0)}{k_z^{\mathrm{atm}}}\right) \frac{\cosh[jk_z^{\mathrm{atm}}(z+d)]}{\sinh[jk_z^{\mathrm{atm}}(d)]}e^{j(k_x x+k_y y)}, \tag{19}$$

assuming that $k_x^2+k_y^2 > \frac{\omega^2}{c^2}$. Substituting Eq. (17) to Eq. (19) and Eq. (15) into Eq. (4) using Eq. (7) gives

$$\Theta^r \begin{bmatrix} \alpha^r \\ \beta^r \end{bmatrix} = \Theta^i \begin{bmatrix} \alpha^i \\ \beta^i \end{bmatrix}, \tag{20}$$

where Θ^i and Θ^r are 2 by 2 matrices of the form

$$\Theta = \begin{bmatrix} a & b \\ c & d \end{bmatrix} \tag{21}$$

for

$$a = S_{11}\,\hat{P}_{x,a} + S_{12}\,\hat{P}_{y,a} - \frac{\hat{P}_{z,a}\,k_x}{\omega} + \frac{\hat{P}_{x,a}\,k_{z,a}}{\omega} + \frac{k_x\xi_{z,a}}{\omega}\coth(-|k_z^{\mathrm{atm}}|d) - \frac{k_z^{\mathrm{atm}}\,\hat{P}_{x,a}}{\omega}\coth(-|k_z^{\mathrm{atm}}|d) \tag{22}$$

$$b = S_{11}\ \hat{P}_{x,f} + S_{12}\ \hat{P}_{y,f} - \frac{\hat{P}_{z,f}\ k_x}{\omega} + \frac{\hat{P}_{x,f}\ k_{z,f}}{\omega} +$$

$$\frac{k_x \xi_{z,f}}{\omega}\coth(-|k_z^{\rm atm}|d) - \frac{k_z^{\rm atm}\ \hat{P}_{x,f}}{\omega}\coth(-|k_z^{\rm atm}|d) \qquad (23)$$

$$c = S_{21}\ \hat{P}_{x,a} + S_{22}\ \hat{P}_{y,a} - \frac{\hat{P}_{z,a}\ k_y}{\omega} + \frac{\hat{P}_{y,a}\ k_{z,a}}{\omega} +$$

$$\frac{k_y \xi_{z,a}}{\omega}\coth(-|k_z^{\rm atm}|d) - \frac{k_z^{\rm atm}\ \hat{P}_{y,a}}{\omega}\coth(-|k_z^{\rm atm}|d) \qquad (24)$$

$$d = S_{21}\ \hat{P}_{x,f} + S_{22}\ \hat{P}_{y,f} - \frac{\hat{P}_{z,f}\ k_y}{\omega} + \frac{\hat{P}_{y,f}\ k_{z,f}}{\omega} +$$

$$\frac{k_y \xi_{z,f}}{\omega}\coth(-|k_z^{\rm atm}|d) - \frac{k_z^{\rm atm}\ \hat{P}_{y,f}}{\omega}\coth(-|k_z^{\rm atm}|d), \qquad (25)$$

where $\xi_{z,a} = -(k_x\ \hat{P}_{x,a} + k_y\ \hat{P}_{y,a})/k_z^{\rm atm}$ and $\xi_{z,f} = -(k_x\ \hat{P}_{x,f} + k_y\ \hat{P}_{y,f})/k_z^{\rm atm}$. The Θ^i and Θ^r matrices depend on whether the wave is incident or reflected from the ionosphere. Vertical wave numbers for the fast and shear Alfvén modes and the vertical wave number in the atmosphere are $k_{z,f}$, $k_{z,a}$ and $k_z^{\rm atm}$, respectively. The $S_{i,j}$ represent terms involving the height integrated conductivities of the ionosphere that are required for the wave magnetic field boundary condition at the ionosphere for an oblique $\boldsymbol{B_0}$. Further details are given in the context of Eqs. (12) and (13) of Sciffer and Waters (2002). Note that the expressions for the $S_{i,j}$ in Sciffer and Waters (2002, their Eqs. 41–44) contain some typographic errors. All the plus signs should be minus signs and the appropriate sign correction applied to their Eqs. (12) and (13). Furthermore, the expressions for a, b, c and d should contain the hyperbolic cotangent function, as given above, while the equivalent expressions in Waters and Sciffer (2002) incorrectly contain the hyperbolic tangent function. These corrections do not affect the results presented in the figures of Sciffer and Waters (2002).

From Eq. (20), the amplitudes of the reflected MHD modes are

$$\begin{bmatrix}\alpha^r\\ \beta^r\end{bmatrix} = \left(\Theta^r\right)^{-1}\Theta^i\begin{bmatrix}\alpha^i\\ \beta^i\end{bmatrix} = \begin{bmatrix}\Gamma_{11}\ \Gamma_{12}\\ \Gamma_{21}\ \Gamma_{22}\end{bmatrix}\begin{bmatrix}\alpha^i\\ \beta^i\end{bmatrix}. \qquad (26)$$

In terms of Eqs. (22)–(25),

$$\begin{bmatrix}\Gamma_{11}\ \Gamma_{12}\\ \Gamma_{21}\ \Gamma_{22}\end{bmatrix} = \frac{1}{a^r d^r - b^r c^r}\begin{bmatrix} a^i d^r - c^i b^r & b^i d^r - d^i b^r\\ -a^i c^r + c^i a^r & -b^i c^r + d^i a^r\end{bmatrix}, \qquad (27)$$

where the subscripts r and i identify the reflected and incident forms of a, b, c and d.

The 2 by 2, reflection and mode conversion coefficient matrix (RCM), defined by Eq. (27), contains the elements Γ_{ij}, which describe the reflection and mode conversion properties of ULF waves for the combined magnetosphere/ionosphere/atmosphere/ground system. The elements of the RCM are defined by Eqs. (22)–(25) and Eq. (26). The contribution of the incident shear Alfvén mode in the reflected shear Alfvén mode is determined by Γ_{11}, the contribution of the incident fast mode in the reflected shear Alfvén mode is determined by Γ_{12}, and so on. They all depend on dip angle, the three ionospheric conductivities, ULF disturbance wave numbers, wave frequency and the height of the ionospheric current sheet above the ground. Experimental quantities are the electric and/or magnetic field perturbations which must be constructed using both Eq. (15) and Eq. (26). The explicit expressions are developed below. Note that the elements, Γ_{ij} are complex and contain phasing information for the incident and reflected waves.

3 Electric and magnetic fields in the magnetosphere and atmosphere

For a given α^i and β^i, α^r and β^r may be calculated for a specific set of wave parameters and ionosphere conditions from Eq. (26). For sinusoidal temporal dependence, the electric fields as a function of altitude in the magnetosphere are

$$e_x^m(z) = \alpha^r\ \hat{P}^r_{x,a}\ e^{j(k^r_{z,a})z} + \alpha^i\ \hat{P}^i_{x,a}\ e^{j(k^i_{z,a})z} + \beta^r\ \hat{P}^r_{x,f}\ e^{j(k^r_{z,f})z} + \beta^i\ \hat{P}^i_{x,f}\ e^{j(k^i_{z,f})z} \qquad (28)$$

$$e_y^m(z) = \alpha^r\ \hat{P}^r_{y,a}\ e^{j(k^r_{z,a})z} + \alpha^i\ \hat{P}^i_{y,a}\ e^{j(k^i_{z,a})z} + \beta^r\ \hat{P}^r_{y,f}\ e^{j(k^r_{z,f})z} + \beta^i\ \hat{P}^i_{y,f}\ e^{j(k^i_{z,f})z} \qquad (29)$$

$$e_z^m(z) = \alpha^r\ \hat{P}^r_{z,a}\ e^{j(k^r_{z,a})z} + \alpha^i\ \hat{P}^i_{z,a}\ e^{j(k^i_{z,a})z} + \beta^r\ \hat{P}^r_{z,f}\ e^{j(k^r_{z,f})z} + \beta^i\ \hat{P}^i_{z,f}\ e^{j(k^i_{z,f})z} \qquad (30)$$

The k_z now have i and r identifiers which relate to the $\pm$ sign choice in Eq. (9) and Eq. (13). For the fast mode, take the plus sign in Eq. (9) for $k^r_{z,f}$ and the minus sign for $k^i_{z,f}$. The k_z for the shear Alfvén mode also depends on the direction of $\boldsymbol{B_0}$. For the Northern Hemisphere, take the plus sign in Eq. (13) for $k^i_{z,a}$ and the minus sign for $k^r_{z,a}$. These are reversed for the Southern Hemisphere.

The electric fields in the atmosphere, as a function of height, are

$$e_x^{\rm atm}(z) = e_x^m(0)\frac{\sinh[jk_z^{\rm atm}(z+d)]}{\sinh[jk_z^{\rm atm}(d)]} \qquad (31)$$

$$e_y^{\rm atm}(z) = e_y^m(0)\frac{\sinh[jk_z^{\rm atm}(z+d)]}{\sinh[jk_z^{\rm atm}(d)]} \qquad (32)$$

$$e_z^{\rm atm}(z) = \left(\frac{-k_x e_x^m(0) - k_y e_y^m(0)}{k_z^{\rm atm}}\right)\frac{\cosh[jk_z^{\rm atm}(z+d)]}{\sinh[jk_z^{\rm atm}(d)]}. \qquad (33)$$

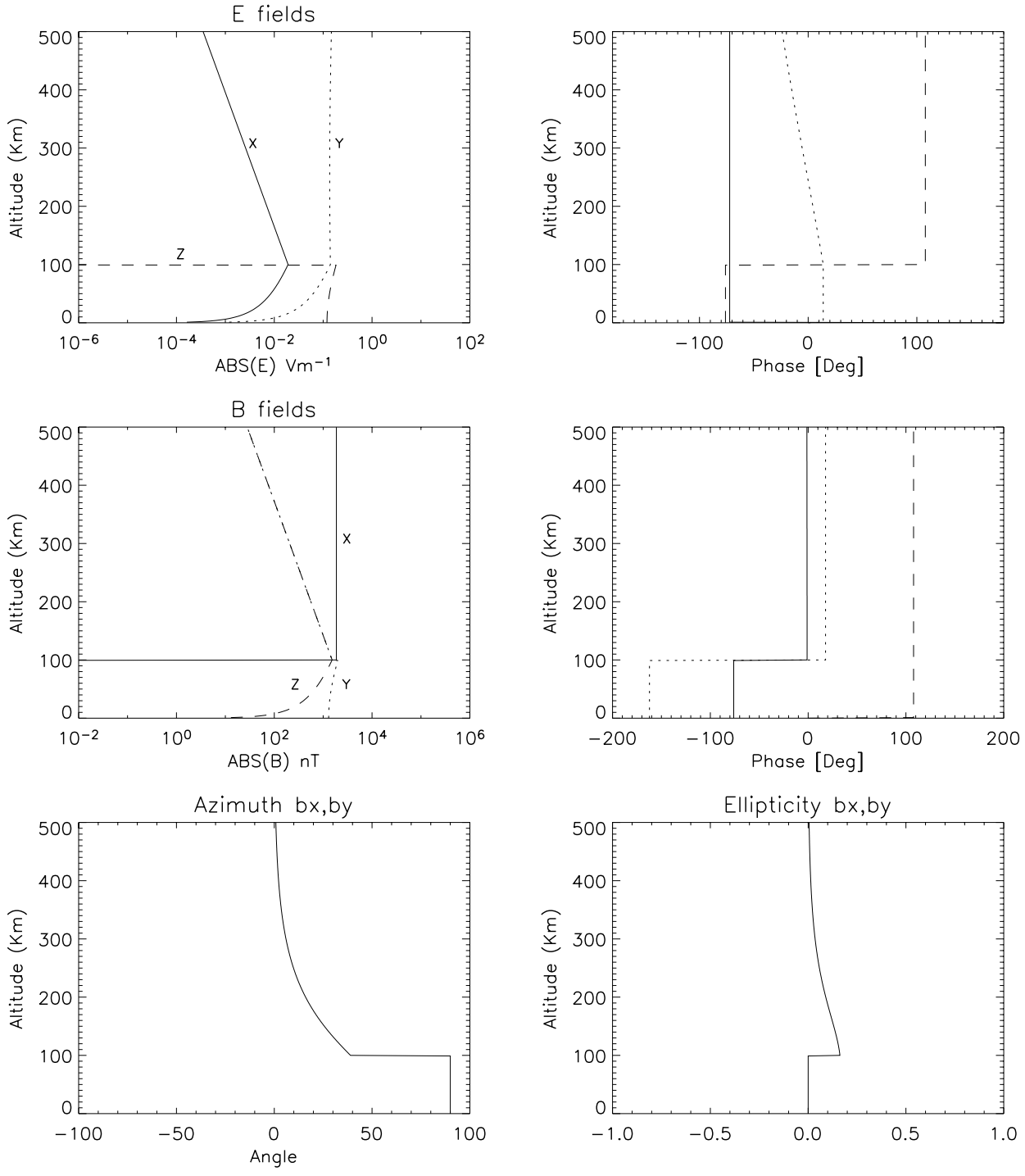

Fig. 2. ULF wave fields for vertical $\boldsymbol{B_0}$, k_x=0, k_y=1/d, d=100 km, V_a=1×10^6 ms^{-1}, f=20 mHz, α_P=10 and α_H=20. The wave fields are X (solid), Y (dotted) and Z (dashed). The azimuth panel shows the NDR.

The magnetic field components in each region may be calculated using Eqs. (28) to (33) in Eq. (7). For the magnetosphere ($z>0$)

$$b_x^m(z) = \frac{k_y}{\omega} e_z^m(z) - \frac{k_{z,a}^r}{\omega} e_{y,a}^{m,r}(z) - \frac{k_{z,a}^i}{\omega} e_{y,a}^{m,i}(z) - \frac{k_{z,f}^r}{\omega} e_{y,f}^{m,r}(z) - \frac{k_{z,f}^i}{\omega} e_{y,f}^{m,i}(z) \tag{34}$$

$$b_y^m(z) = -\frac{k_x}{\omega} e_z^m(z) + \frac{k_{z,a}^r}{\omega} e_{x,a}^{m,r}(z) + \frac{k_{z,a}^i}{\omega} e_{x,a}^{m,i}(z) + \frac{k_{z,f}^r}{\omega} e_{x,f}^{m,r}(z) + \frac{k_{z,f}^i}{\omega} e_{x,f}^{m,i}(z) \tag{35}$$

$$b_z^m(z) = +\frac{k_x}{\omega}e_y^m(z) - \frac{k_{y,a}^r}{\omega}e_x^m(z). \quad (36)$$

In the atmopshere ($-d \le z < 0$), the magnetic fields are

$$b_x^{\rm atm}(z) = \frac{1}{\omega}[k_y e_z^{\rm atm}(0) -$$

$$k_z^{\rm atm} e_y^{\rm atm}(0)]\frac{\cosh[jk_z^{\rm atm}(z+d)]}{\sinh[jk_z^{\rm atm}(d)]} \quad (37)$$

$$b_y^{\rm atm}(z) = \frac{1}{\omega}[-k_x e_z^{\rm atm}(0) +$$

$$k_z^{\rm atm} e_x^{\rm atm}(0)]\frac{\cosh[jk_z^{\rm atm}(z+d)]}{\sinh[jk_z^{\rm atm}(d)]} \quad (38)$$

$$b_z^{\rm atm}(z) = b_z^m(0)\frac{\sinh[jk_z^{\rm atm}(z+d)]}{\sinh[jk_z^{\rm atm}(d)]} \quad (39)$$

4 Vertical background magnetic field

In order to introduce the expressions for the electric and magnetic wave fields, we begin with a vertical $\boldsymbol{B_0}$ and illustrate the NDR effect described by Hughes (1974). Given an incident shear Alfveń wave with k_x=0 and k_y=$1/d$, the solutions for the electric and magnetic wave fields are shown in Fig. 2. The incident wave consists of e_y and b_x. Interaction with the ionosphere/atmosphere results in wave reflection and the resulting ionosphere current system gives rise to a fast mode wave. The evanescent reflected fast mode is seen in the e_x, b_y and b_z components. Therefore, since β^i=0 for this case, only Γ_{11} and Γ_{21} in the RCM are relevant and as we shall see, Γ_{21} influences the amplitude of the signal seen at the ground. Above 500 km, the magnetic signal is the b_x component, while at the ground, b_y is the larger component. The 90° rotation in wave polarisation azimuth develops over a range of altitudes. This altitude range depends on the vertical wave number of the fast mode. All these features are consistent with the NDR effect described by Hughes (1974).

We now consider the ISE as described by Yoshikawa and Itonaga (1996, 2000) and Yoshikawa et al. (2002), who formulated their solutions for a vertical $\boldsymbol{B_0}$. When I=±90°, Eqs. (22)–(25) simplify to

$$a = \Sigma_P + \Sigma_a \quad (40)$$

$$b = \mp\Sigma_H \quad (41)$$

$$c = \pm\Sigma_H \quad (42)$$

$$d = \Sigma_P + \Sigma_f - \Sigma_{\rm atm}\coth(-|k_z^{\rm atm}|d). \quad (43)$$

For a vertical $\boldsymbol{B_0}$ the Γ_{ij} are constant for a given $k_\perp$. We have chosen k_x=0 and set k_y=$1/d$, where d=100 km, the ionosphere height. These parameters are similar to those found in Yoshikawa et al. (2002), where Σ_P and Σ_H are the height integrated Pedersen and Hall conductivities, Σ_a=$\frac{1}{\mu_0 V_a}$ and Σ_f=$(\sqrt{\frac{\omega^2}{V_a{}^2}-k_\perp^2})/\mu_0\omega$ are the shear Alfvén and fast mode wave conductances, and $\Sigma_{\rm atm}$=$(\sqrt{\frac{\omega^2}{c^2}-k_\perp^2})/\mu_0\omega$ is the wave conductance in the atmosphere. The expression involving our wave mode conversion matrix in Eqs. (26) and (27) can be shown to be equivalent to Eq. (9) in Yoshikawa and Itonaga (1996). Rewriting Eq. (26) in a form that combines our formulation with Yoshikawa and Itonaga (1996) gives

$$\begin{bmatrix}\alpha^r\\ \beta^r\end{bmatrix} = \begin{bmatrix}\Gamma_{11} & (1+\Gamma_{22})\Gamma_{FA}\\ (1+\Gamma_{11})\Gamma_{AF} & \Gamma_{22}\end{bmatrix}\begin{bmatrix}\alpha^i\\ \beta^i\end{bmatrix}, \quad (44)$$

where

$$\Gamma_{11} = \frac{\Sigma_a - \Sigma_a^{\rm eff}}{\Sigma_a + \Sigma_a^{\rm eff}} \quad (45)$$

$$\Gamma_{22} = \frac{\Sigma_f + \Sigma_f^{\rm eff}}{\Sigma_f - \Sigma_f^{\rm eff}} \quad (46)$$

$$\Sigma_a^{\rm eff} = \Sigma_P\left(1 - \frac{\Sigma_H}{\Sigma_P}\Gamma_{AF}\right) \quad (47)$$

$$\Sigma_f^{\rm eff} = \Sigma_P\left[1 - \frac{\Sigma_H}{\Sigma_P}\Gamma_{FA} + \frac{\Sigma_{\rm atm}}{\Sigma_P}\coth(-|k_z^{\rm atm}|d)\right] \quad (48)$$

$$\Gamma_{FA} = \left(\frac{\Sigma_H}{\Sigma_P + \Sigma_a}\right) \quad (49)$$

$$\Gamma_{AF} = \left[\frac{\Sigma_H}{(\Sigma_f - \Sigma_P + \Sigma_{\rm atm}\coth(-|k_z^{\rm atm}|d)}\right]. \quad (50)$$

This is for the case where the fast mode is evanescent in the vertical direction. The reflection and mode conversion coefficients for a propagating fast mode were discussed by Sciffer and Waters (2002).

Yoshikawa and Itonaga (1996, 2000) formulated the problem of the interaction of ULF waves with the ionosphere in terms of the rotation (or curl) and divergence of the ULF wave electric fields. They used $(\nabla\times\boldsymbol{e})_\parallel$ to represent the fast mode and $\nabla\cdot\boldsymbol{e}$ to represent the shear Alfvén mode in the magnetosphere. One useful property of the electric fields of these two ideal MHD wave modes, for a vertical $\boldsymbol{B_0}$, is their orthogonality, i.e. $\boldsymbol{e}_{\rm alfvén}\cdot\boldsymbol{e}_{\rm fast}$=0 (Cross, 1988). Therefore, once the horizontal wave structure (k_x and k_y) is specified and since $e_\parallel$=e_z=0 in the ideal MHD medium, the electric field vectors for the two wave modes are immediately known. These are the $\boldsymbol{P}_a$ and $\boldsymbol{P}_f$ in our formulation introduced in Eqs. (11) and (14). These vectors are the fundamental link between our model and that of Yoshikawa and Itonaga (1996, 2000) for a vertical $\boldsymbol{B_0}$. A formulation based on the divergence and curl of the electric fields is useful in describing high latitude regions, where $\boldsymbol{B_0}$ is near vertical and the formulation emphasises field-aligned currents. For oblique $\boldsymbol{B_0}$, the expressions for the elements of the RCM are more complicated, and the divergence and curl terms are interlinked for a given wave mode.

The ISE for various ULF wave frequencies was illustrated in Fig. 1 of Yoshikawa et al. (2002). Their particular interest

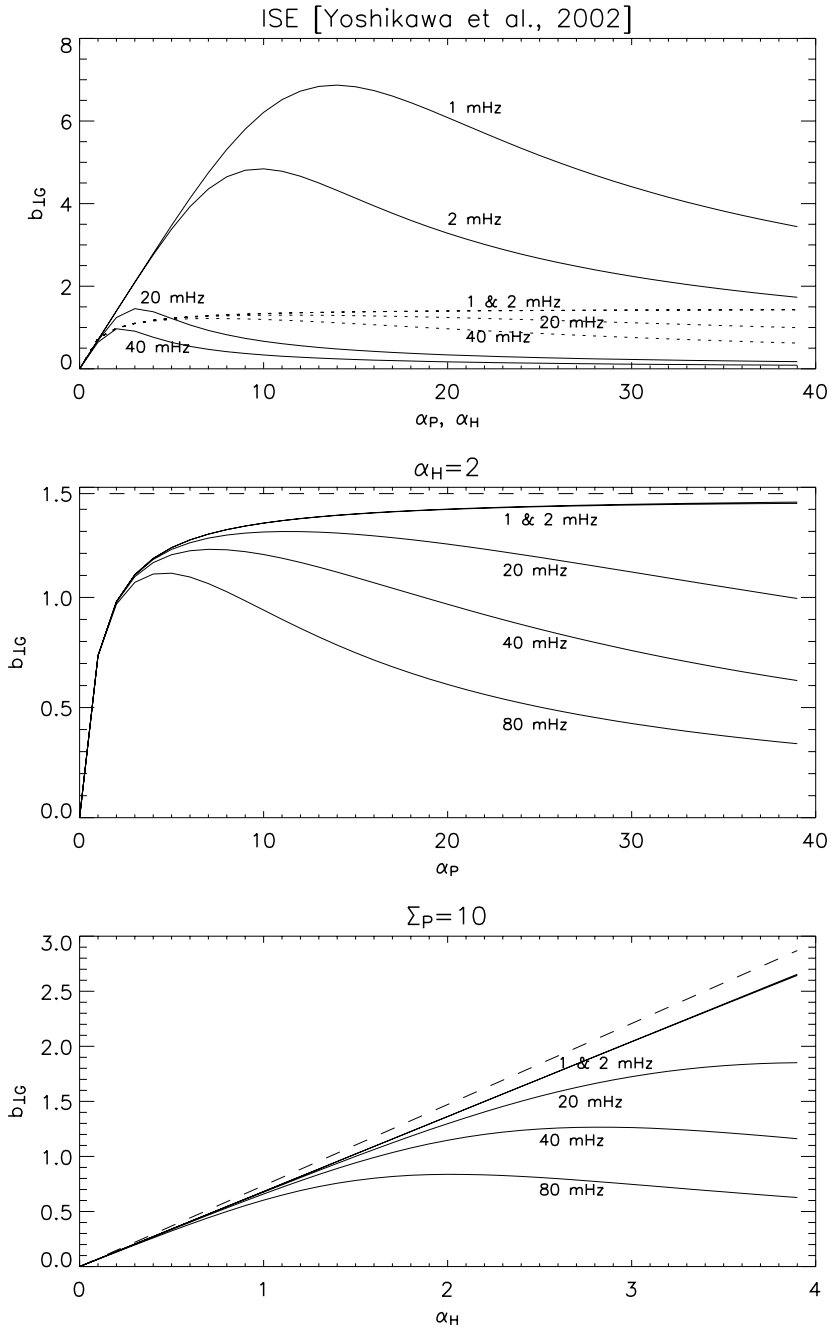

Fig. 3. The normalised, horizontal ULF magnetic field at the ground for vertical $\boldsymbol{B_0}$, V_a=1×10^6 ms^{-1}, k_x=0, k_y=1/d and d=100 km. **(a)** variation with α_P (dotted) and α_H (solid) for the parameters in Yoshikawa et al. (2002). **(b)** Variation with α_P for α_H=2. **(c)** Variation with α_H for Σ_P=10 S.

was to show the variation of the reduction in ULF wave amplitude at the ground as a function of the Pedersen and Hall conductivities. From the parameters given in Yoshikawa et al. (2002), the ground level magnetic field magnitude as a function of α_P and α_H for our model can be found from the equations in Sects. 2 and 3. For an incident shear Alfvén mode wave we set β^i=0. With I=90°, k_x=0, k_y=1/d and α^i=1, we find that $\overset{\wedge i}{P}_{x,f} = \overset{\wedge r}{P}_{x,f}$ =1 and $\overset{\wedge i}{P}_{y,a} = \overset{\wedge r}{P}_{y,a}$ =1 are the only nonzero terms from Eqs. (11) and (14). From Eqs. (37) to (39) we obtain $b_{x(z=-d)}$=$b_{z(z=-d)}$=0 and

$$b_{y(z=-d)} = \frac{jk_y}{\omega}\left[(1+\Gamma_{11})\,\Gamma_{AF}\right]\frac{2\mu_0 V_A}{e^{-1}-e}, \tag{51}$$

which shows the dependence of the ground magnetic field on Γ_{11} and Γ_{AF}. Figure 3a shows how Eq. (51) varies with both α_P and α_H for wave frequencies of 1, 2, 20 and 40 mHz. The amplitude has been normalised by the incident wave

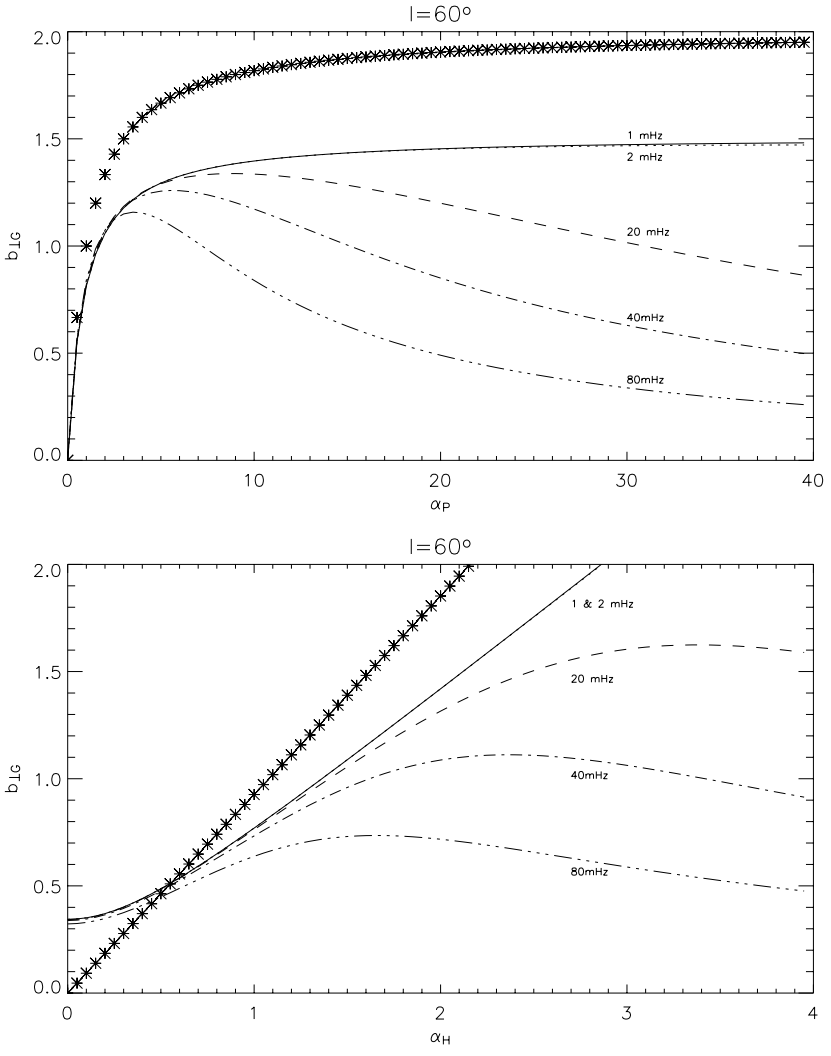

Fig. 4. The normalised, horizontal ULF magnetic field at the ground for a $\boldsymbol{B_0}$ dip angle of 60°, V_a=1×10^6 ms^{-1}, k_x=0, k_y=1/d and d=100 km. **(a)** Variation with α_P for α_H=2. **(b)** Variation with α_H for Σ_P=10 S. The * symbols show the $\frac{\Sigma_H}{\Sigma_p+\Sigma_a}$ curve.

magnetic field magnitude just above the ionospheric current sheet. Following Yoshikawa et al. (2002), $|k_\perp|d$=1, α_H=2 for variations with α_P (dotted curves) and α_P=20 for variations with α_H (solid curves). The ISE is small for small Γ_{AF} which makes Eq. (45) equal to Eq. (1) as $\Gamma_A^{\rm eff}\approx\Sigma_P$. Therefore, the electrostatic limit may be achieved by reducing Σ_H, increasing $k_\perp$ and/or reducing ω which increases both Σ_f and $\Sigma_{\rm atm}$. For a vertical $\boldsymbol{B_0}$, our Γ_{AF} is related to the inductive process of Yoshikawa and Itonaga (2000) by

$$\Gamma_{AF} = \frac{\nabla \times \boldsymbol{e}_\perp^I}{\nabla \bullet \boldsymbol{e}_\perp^I} \tag{52}$$

which is small in the electrostatic limit. Figure 3a shows that the ISE is more pronounced for variations with α_H. However, since α_P=20 for this case and $\Sigma_a\approx$0.8, even at α_H=10 the values for Σ_H are much larger than would be typically observed. A comparison that is more representative of middle to low latitudes is shown in Figs. 3b and 3c. The dashed lines show the values for the electrostatic approximation in Eq. (2). For example, for Fig. 3b, Σ_H/Σ_P=2 so $2\alpha_H\, e^{-1}$=1.47 and the low frequencies approach the electrostatic limit for increasing α_P. In Figs. 3b and 3c, the $\frac{\Sigma_H}{\Sigma_P+\Sigma_a}$ term in Eq. (3) follows close to the 1 and 2 mHz curves. The decrease in amplitude for the higher frequencies is due to the ISE. All features of Fig. 3 are consistent with Yoshikawa et al. (2002).

5 Oblique background magnetic field

The formulation in Yoshikawa and Itonaga (1996, 2000) is based on the divergence and curl of the electric fields in the ionosphere which are matched to the divergent and rotational terms in the magnetosphere through the continuity of horizontal electric fields. The two ULF wave modes in the magnetosphere have orthogonal electric fields and can, therefore, be viewed as an orthogonal basis. For example, computing

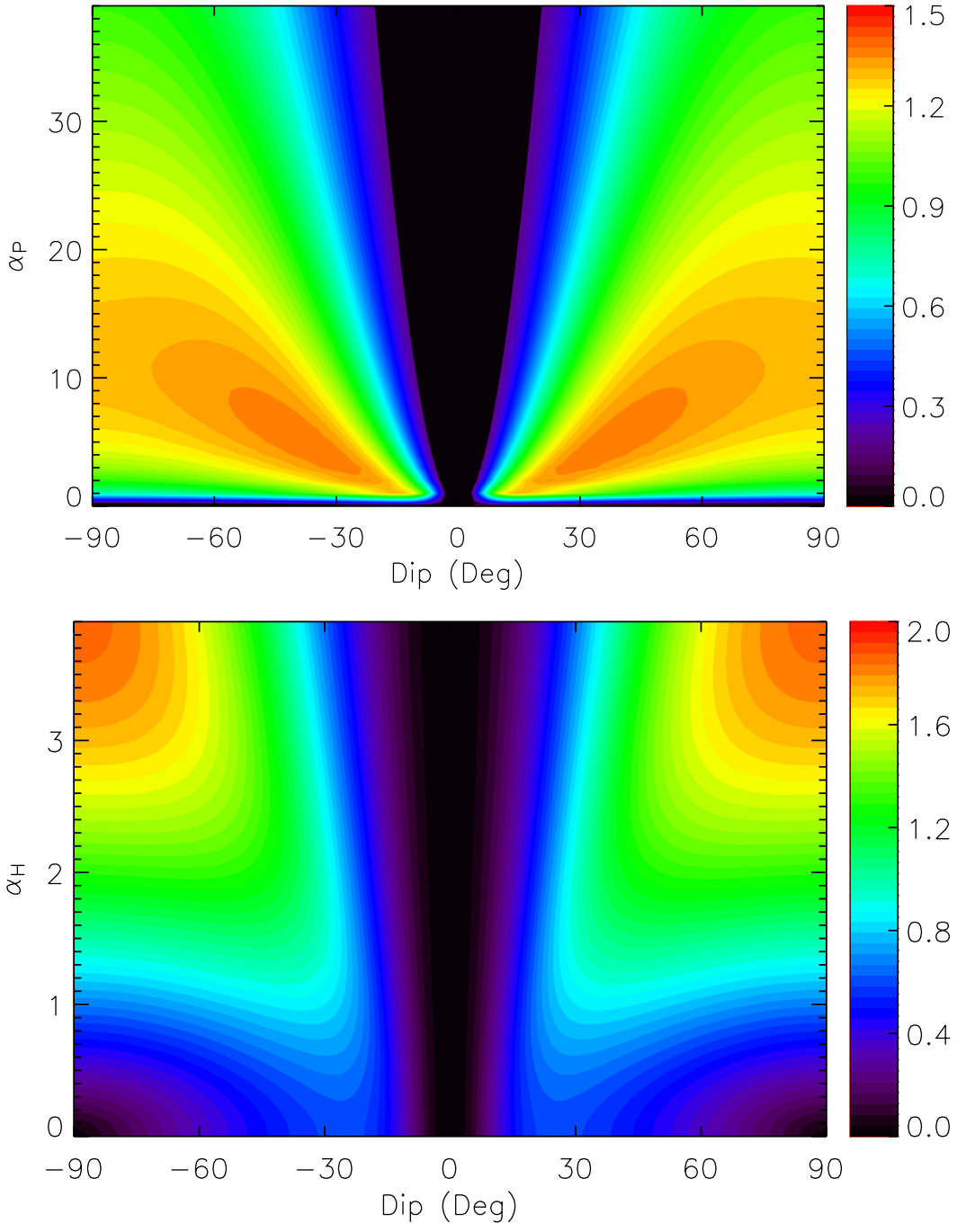

Fig. 5. The normalised, orizontal ULF magnetic field at the ground as a function of dip angle for f=20 mHz, V_a=1×10^6 ms^{-1}, k_x=0, k_y=1/d and d=100 km. **(a)** Variation with α_P for α_H=2. **(b)** Variation with α_H for Σ_P=10 S.

$\nabla\cdot\boldsymbol{e}$ anywhere in the model magnetosphere, ionosphere or atmosphere gives the complex wave amplitude of the shear Alfvén mode part of the solution and $(\nabla\times\boldsymbol{e})_\parallel$ gives the amplitude of the fast mode part of the solution. These are the two parts of the solution used by Hughes (1974).

For oblique $\boldsymbol{B_0}$, the vertical component of the wave electric field is no longer zero. In the magnetosphere, the wave electric field lies in a plane perpendicular to $\boldsymbol{B_0}$ and is no longer parallel to the ionospheric current sheet. The relationship between $\boldsymbol{k}$ and $\boldsymbol{e}$ is contained in the expressions for $\boldsymbol{P}_a$ and $\boldsymbol{P}_f$ which describe the direction of the wave electric field vectors for each wave mode, given the horizontal wave structure, k_x and k_y. In general, $\boldsymbol{P}_a\bullet\boldsymbol{P}_f\neq 0$ for $I\neq\pm 90°$ as the x- and z-components of the shear Alfvén wave electric field and the y component of the fast mode electric field depend on the vertical wave numbers, $k_{z,a}$ and $k_{z,f}$. In general, the angle between the projections of the fast and shear Alfvén mode electric fields onto the ionospheric current sheet (XY plane)

is not 90°. It is the projection of $\boldsymbol{P}_a$ and $\boldsymbol{P}_f$ onto the XY plane which is used in our electric field continuity boundary conditon rather than the rotation (or curl) and divergence of the electric fields.

The discontinuity in e_z across the ionospheric current sheet is related to a net charge density. An oblique $\boldsymbol{B_0}$ gives a nonzero, vertical component of the electric field in the ionosphere current sheet. This is contained in the S_{ij} terms in Eqs. (22) to (25). For the thin current sheet approximation, the constraint in the ionosphere is on the current density whereby J_z^I=0. The formulation in Yoshikawa and Itonaga (1996, 2000) does not need to consider $e_z^I \neq 0$. These differences add complexitites from cross-coupled and additional terms in the equations, as can be appreciated by comparing Eqs. (41)–(43) for a vertical $\boldsymbol{B_0}$ compared with Eqs. (22)–(25) for the oblique $\boldsymbol{B_0}$ case.

The mathematical development in Sects. 2 and 3 allows for the investigation of the interaction of ULF waves with an idealised magnetosphere/ionosphere/ground system for oblique $\boldsymbol{B_0}$ in a 1-D geometry. There are many parameters that can be varied, and their interdependence was discussed to some extent in Sciffer and Waters (2002). In this paper, we focus on the ISE, extending the work of Yoshikawa and Itonaga (1996, 2000) for middle to low latitudes. Keeping the parameters in Fig. 3 (k_x=0, k_y=1/d, d=1×10^5 m and V_a=1×10^6 ms^{-1}), the ground level, normalised horizontal magnetic wave field magnitude ($b_{\perp G}$) as a function of conductivity is shown in Fig. 4 for a dip angle of 60°. The values for $b_{\perp G}$ are computed as the magnitude of the horizontal wave magnetic field at the ground divided by the magnitude of the incident wave magnetic field just above the ionospheric current sheet. Comparing Fig. 4 with Fig. 3 shows that the variation of $b_{\perp G}$ with α_P for a dip angle of 60° is similar to the vertical $\boldsymbol{B_0}$ case. The maximum in $b_{\perp G}$, seen for 20, 40 and 80 mHz, moves to smaller values of α_P and becomes more pronounced as the dip angle decreases (lower latitudes). The variation of $b_{\perp G}$ with α_H shows more dramatic differences when compared with the vertical $\boldsymbol{B_0}$ case. An oblique $\boldsymbol{B_0}$ introduces a nonzero $b_{\perp G}$ for zero Hall conductivity. This effect shows that an oblique FAC can be detected at the ground due to the horizontal FAC component, even in the electrostatic limit as discussed by Tamao (1986). For the higher frequencies (20, 40 and 80 mHz), an oblique $\boldsymbol{B_0}$ reduces the maximum of $b_{\perp G}$ and shifts the maximum to smaller values of α_H.

The effects of the $\boldsymbol{B_0}$ dip angle on the normalised magnitude of $b_{\perp G}$ at 20 mHz are shown in Fig. 5. Vertical slices at 90° and 60° correspond with Figs. 3 and 4 for 20 mHz. Figure 5a shows the variation of $b_{\perp G}$ with α_P, where the maximum in $b_{\perp G}$ moves to smaller values of α_P as the dip angle decreases. As the frequency increases, $b_{\perp G}$ decreases and the higher latitude peak in $b_{\perp G}$ is pushed to smaller values of α_P. For example, for 40 mHz, the peak in $b_{\perp G}$ at 70° is for $\alpha_P \approx 7$. The variation of $b_{\perp G}$ with α_H is shown in Fig. 5b. As the dip angle decreases, $b_{\perp G}$ depends less on α_H until at some latitude (which depends on the parameters chosen), $b_{\perp G}$ becomes independent of α_H.

6 Discussion

The ionosphere represents an inner boundary for ULF waves in the Earth's magnetosphere. A first approximation for treating ULF wave interactions with the ionosphere is to set the wave electric fields to zero and ignore wave mode conversion. Effects of the ionosphere-ground system on ULF wave properties might be considered negligible, considering the wavelengths of typical ULF disturbances compared with the ionosphere's thickness and height. However, previous studies show that ULF wave properties deduced from ground-based measurements must allow for modifications introduced by the ionosphere, even for the simpler case when $\boldsymbol{B_0}$ is vertical and the ionosphere is horizontally uniform. The expressions developed in Sects. 2 and 3 show that the interaction of ULF waves with the ionosphere is nontrivial and depends on the $\boldsymbol{B_0}$ dip angle. While there are a number of modifications to ULF wave properties introduced by the ionosphere, the effects due to the inductive response to time varying currents have recently been explored by Yoshikawa and Itonaga (1996, 2000). In the following discussion, we focus on this inductive aspect of the system in the context of oblique $\boldsymbol{B_0}$.

The variation in the magnitude of ULF magnetic perturbations at ground level as a function of conductivity and dip angle are evident in Figs. 4 and 5. An appreciation of the physical processes causing these effects may be gained by examining the ionospheric current density, the source of these magnetic fields. The essential difference between an electrostatic compared with an inductive ionosphere is seen by comparing the divergence and curl of the ionospheric current density, $\boldsymbol{J}^I$, for the two cases (Yoshikawa and Itonaga, 2000). For a horizontally uniform electrostatic ionosphere with vertical $\boldsymbol{B_0}$

$$\nabla \cdot \boldsymbol{J}^I = \Sigma_P \nabla \cdot \boldsymbol{e}^I \tag{53}$$

$$(\nabla \times \boldsymbol{J}^I)_\parallel = \Sigma_H \nabla \cdot \boldsymbol{e}^I. \tag{54}$$

In this electrostatic approximation, Eq. (54) is the source of the magnetic field perturbation detected on the ground. For the inductive ionosphere, Yoshikawa and Itonaga (2000) added the inductive terms to give

$$\nabla \cdot \boldsymbol{J}^I = \Sigma_P \nabla \cdot \boldsymbol{e}^I - \Sigma_H (\nabla \times \boldsymbol{e}^I)_\parallel \tag{55}$$

$$(\nabla \times \boldsymbol{J}^I)_\parallel = \Sigma_H \nabla \cdot \boldsymbol{e}^I + \Sigma_P (\nabla \times \boldsymbol{e}^I)_\parallel. \tag{56}$$

The divergence of the current density involves both a divergence and curl of the electric field, as does the curl of the current density. The two additional "inductive" currents, $\Sigma_H(\nabla \times \boldsymbol{e}^I)_\parallel$ and $\Sigma_P(\nabla \times \boldsymbol{e}^I)_\parallel$, were identified as the divergent Hall current and the rotational Pedersen current, respectively.

For oblique $\boldsymbol{B_0}$, the divergence and curl of the current density in the ionosphere (J_z=0) can be found from Eq. (6) and the electric field boundary conditions and are given by

$$\nabla \cdot \boldsymbol{J}^I = S_1 \nabla \cdot \boldsymbol{e}^I - S_2 (\nabla \times \boldsymbol{e}^I)_z + S_3 \frac{\partial e_y}{\partial y}, \tag{57}$$

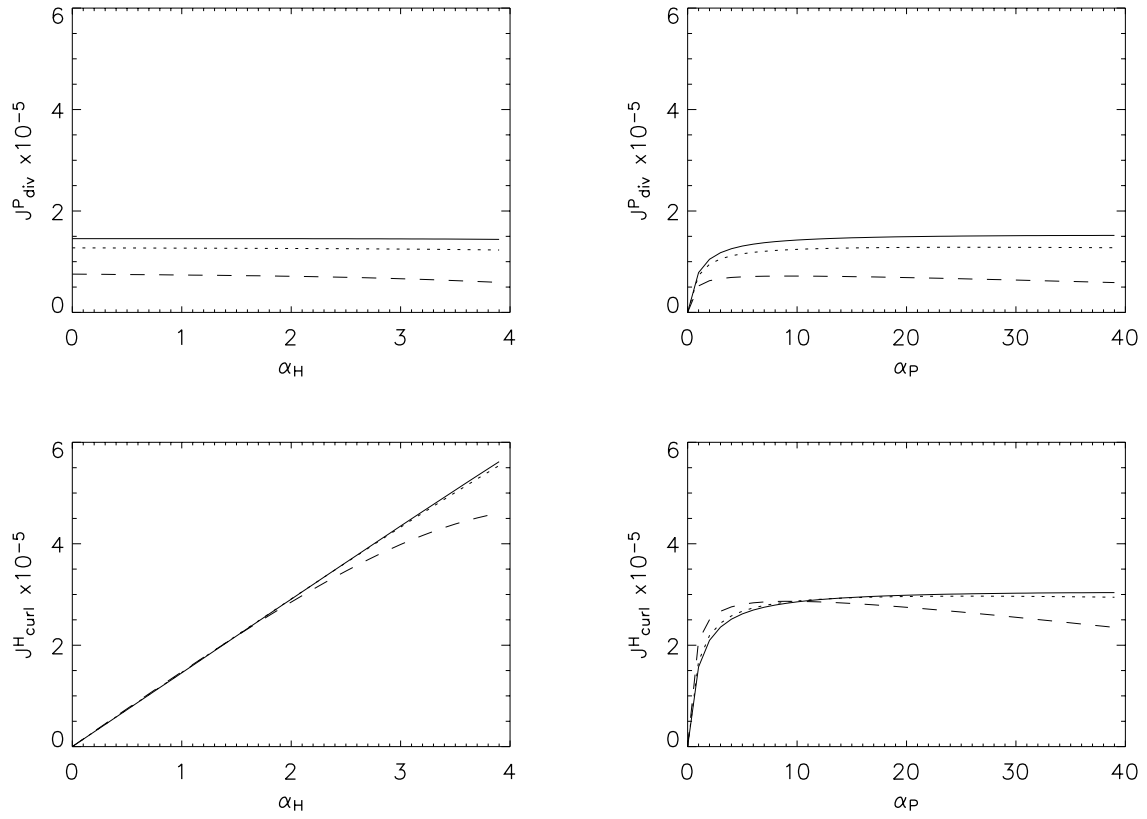

Fig. 6. The magnitude of the ionospheric current densities for the electrostatic approximation where V_a=1×10^6 ms^{-1}, k_x=0, k_y=1/d and d=100 km and f=2 mHz. The variation with α_P has α_H=2 and the variation with α_H has Σ_P=10 S. The dip angle of $\boldsymbol{B_0}$ is 90° (solid), 60° (dotted) and 30° (dashed) lines.

which is equivalent to

$$\nabla \cdot \boldsymbol{J}^I = S_4 \nabla \cdot \boldsymbol{e}^I - S_2 (\nabla \times \boldsymbol{e}^I)_z - S_3 \frac{\partial e_x}{\partial x} \tag{58}$$

and the curl equations for oblique $\boldsymbol{B_0}$ are

$$(\nabla \times \boldsymbol{J}^I)_z = S_2 \nabla \cdot \boldsymbol{e}^I + S_1 (\nabla \times \boldsymbol{e}^I)_z - S_3 \frac{\partial e_y}{\partial x}, \tag{59}$$

which is equivalent to

$$(\nabla \times \boldsymbol{J}^I)_z = S_2 \nabla \cdot \boldsymbol{e}^I + S_4 (\nabla \times \boldsymbol{e}^I)_z - S_3 \frac{\partial e_x}{\partial y}, \tag{60}$$

where the various coefficients are

$$S_1 = \frac{\Sigma_P \Sigma_d}{\Sigma_d sin^2 I + \Sigma_P cos^2 I} \tag{61}$$

$$S_2 = \frac{\Sigma_H \Sigma_d sin I}{\Sigma_d sin^2 I + \Sigma_P cos^2 I} \tag{62}$$

$$S_3 = \frac{cos^2 I (\Sigma_P{}^2 + \Sigma_H{}^2 - \Sigma_P \Sigma_d)}{\Sigma_d sin^2 I + \Sigma_P cos^2 I} \tag{63}$$

$$S_4 = S_3 + S_1. \tag{64}$$

These equations are similar to Eqs. (55) and (56), except for one extra term in each of Eqs. (57)–(60) that involves the divergence in Eqs. (57) and (58) and the curl in Eqs. (59) and (60). The S_3 multiplier goes to zero for vertical $\boldsymbol{B_0}$, indicating that the extra terms in Eqs. (57)–(60) arise from the conductivity given by Σ_d in the XZ plane. If either k_x or k_y is zero, then the divergence and curl of J can be expressed so that this extra term is zero. The contribution of the inductive terms in the ionosphere can now be compared with the electrostatic approximation for oblique $\boldsymbol{B_0}$. Following Yoshikawa and Itonaga (2000), for k_x=0 we define the following parts of the current density,

$$\boldsymbol{J}^P_{\rm div} = S_4 \nabla \bullet \boldsymbol{e}^I \tag{65}$$

$$\boldsymbol{J}^H_{\rm curl} = S_2 \nabla \cdot \boldsymbol{e}^I \tag{66}$$

$$\boldsymbol{J}^H_{\rm div} = S_2 (\nabla \times \boldsymbol{e}^I)_z \tag{67}$$

$$\boldsymbol{J}^P_{\rm curl} = S_1 (\nabla \times \boldsymbol{e}^I)_z, \tag{68}$$

where Eqs. (67) and (68) are small in the electrostatic approximation.

The variations of $\boldsymbol{J}^P_{div}$ and $\boldsymbol{J}^H_{curl}$ with α_P and α_H are shown in Fig. 6 for dip angles of 30°, 60° and 90° (vertical). The electrostatic limit has been approximated by using a low frequency of 2 mHz. The 90° curves for $\boldsymbol{J}^H{}_{curl}$ have a similar shape to the low frequency $b_{\perp G}$ variations with α_P

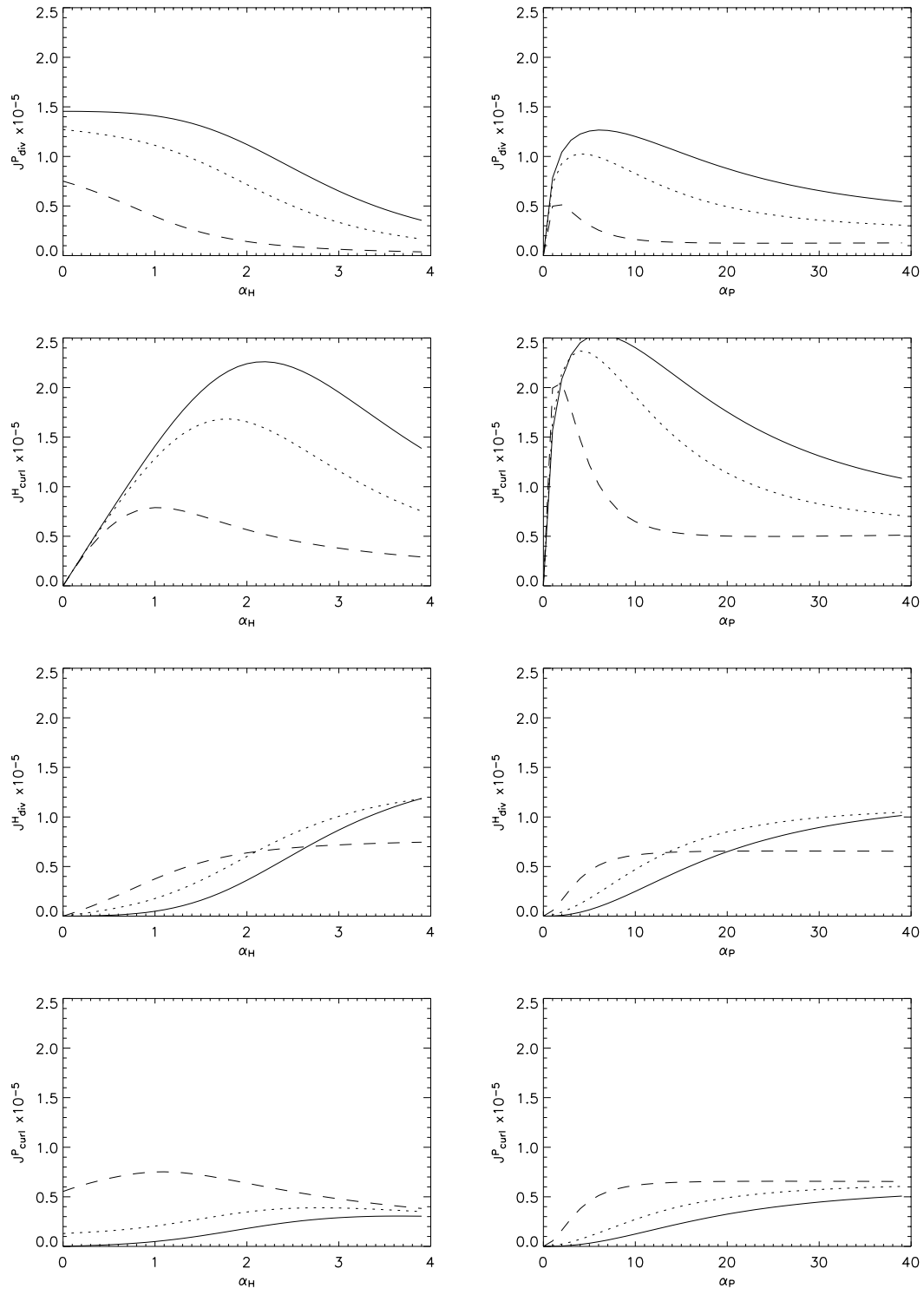

Fig. 7. The magnitude of the ionospheric current densities for the inductive effect where V_a=1×10^6 ms^{-1}, k_x=0, k_y=1/d for d=100 km and f=40 mHz. The variation with α_P has α_H=2 and the variation with α_H has Σ_P=10 S. The dip angle of $\boldsymbol{B_0}$ is 90° (solid), 60° (dotted) and 30° (dashed) lines.

and α_H shown in Figs. 3b and 3c. This is to be expected as the ionosphere Hall current is the source of $b_{\perp\, G}$ in this case. As $\boldsymbol{B_0}$ goes oblique, part of $\boldsymbol{J}^P_{\rm div}$ contributes to the ground field. This is the reason for the nonzero $b_{\perp G}$ when α_H is zero in Fig. 4b.

The magnitude of the inductive terms becomes larger as the frequency is increased. The magnitudes of $\boldsymbol{J}^P_{\rm div}$, $\boldsymbol{J}^H_{\rm curl}$, $\boldsymbol{J}^H_{\rm div}$ and $\boldsymbol{J}^P_{\rm curl}$ with α_P and α_H are shown in Fig. 7 for dip angles of 30°, 60° and 90° (vertical) and for 40 mHz. The solid curves (for 90°) are the same as the ionospheric currents shown in Figs. 11 and 12 of Yoshikawa and Itonaga (2000) but we can now see the effects of oblique $\boldsymbol{B_0}$. The top four panels of Fig. 7 show the magnitude of the ionospheric currents described by the first terms of Eqs. (58) and (59), while the bottom four panels show the magnitudes of the inductive terms.

Consider the top four panels of Fig. 7. The inductive effect feeds back to provide a decrease in magnitude with increasing conductivity, as seen in Yoshikawa and Itonaga (2000). This tends to increase at lower latitudes, where the $\boldsymbol{B_0}$ dip angle is smaller. Three of the 4 top panels that exhibit maxima all show a shift of the maximum in the divergence and curl of the current to smaller values of α_P and α_H for lower latitudes. This effect contributes to the increase in the ULF magnetic field detected on the ground for smaller values of α_P and at lower latitudes, as shown in Fig. 5a.

The lower four panels of Fig. 7 show the magnitude of the inductive terms of Eqs. (58) and (59) with conductivity. The inductive effect for vertical $\boldsymbol{B_0}$ is smaller compared with the 60° dip angle curves. The importance of the ISE at low latitudes is also seen where the inductive terms for the 30° dip angle are larger for $\boldsymbol{J}^P_{curl}$ and dominate for the smaller values of α_P and α_H. The lower latitudes (at 30°) show a "saturation" as the inductive terms remain constant with α_P for $\alpha_P \geq 10$. From the International Reference Ionosphere model (IRI-95), an estimate of the maximum conductivities expected for mid and low latitudes was obtained. For midsummer at 50° geomagnetic latitude at local noon, the height integrated Pedersen and Hall conductivities reached $\approx$20 S with the largest value for $\alpha_H \approx 1.3$. With more typical values of Σ_P=10 S used in Fig. 7, we might expect to see evidence of the ISE at low latitudes, even for $\alpha_H \approx 1$. The ISE also depends on the spatial scale size, k_x and k_y. While azimuthal wave numbers for ULF waves have been estimated using ground-based magnetometer arrays, these do not necessarily translate to similar spatial structure in the ionosphere (Hughes and Southwood, 1976; Ponomarenko et al., 2001). Determining the actual spatial structure of ULF waves incident on the ionosphere is a part of current research. Recent developments in extracting ULF wave signatures from the Super Dual Auroral Radar Network (SuperDARN) (Ponomarenko et al., 2003) promises to reveal the necessary spatial information and allow for comparisons with ground magnetometer signals. This may provide an experimental check on the ISE, if the parameters allow a significant ISE at latitudes where the radars reveal ULF signals.

7 Conclusion

Analytic expressions for ULF wave fields through the ionosphere/atmosphere within the context of oblique $\boldsymbol{B_0}$ have been developed. There are many parameters that contribute to the complex interaction of ULF waves with the ionosphere/atmosphere/ground system. In this paper, we have focussed on the ISE as a function of the $\boldsymbol{B_0}$ dip angle and ionosphere conductivity. In general, as the dip angle decreases (lower latitudes), the maxima in $b_{\perp G}$ moves to smaller values of the ionosphere conductivity. This arises from the combined effects of the ISE and the direct contribution, shown in Fig. 4, where the horizontal component of the FAC associated with an incident shear Alfvén wave directly contributes to the ground fields. The physical processes that determine the magnetic ground signal may be understood from the behavior of the ionospheric currents. Taking the divergence and curl of $\boldsymbol{J}^I$ shows the relative contribution to the ground signal from the conductivity tensor and the ionospheric electric fields.

The variation of the height integrated conductivity tensor with $\boldsymbol{B_0}$ is well known for a horizontally uniform ionosphere. This approximation is adequate for middle to low latitudes. At auroral latitudes, horizontal gradients in the conductivity would need to be included in Eq. (6), a refinement for future work. Solutions for the ULF magnetic and electric wave fields for an oblique $\boldsymbol{B_0}$ have been described and involve the full reflection and conversion coefficient matrix developed in Sciffer and Waters (2002). The model accomodates any polarisation and mix of the shear Alfvén and fast mode MHD waves. While wave mode conversion occurs due to induced currents in the ionosphere, the model assumes that the incident wave structure of coupled modes in the magnetosphere is known. The equations developed in this paper should be useful for coupled magnetosphere/ionosphere ULF wave modeling codes that require realistic ionosphere boundary conditions, including the effects of an oblique $\boldsymbol{B_0}$.

Acknowledgements. This work was supported by the Australian Research Council, the University of Newcastle and the Commonwealth of Australia through the Cooperative Research Centre for Satellite Systems.

Topical Editor M. Lester thanks A. Yoshikawa and D. Wright for their help in evaluating this paper.

References

Alfvén, H. and Fälthammar, C. G.: Cosmical electrodynamics, Oxford University Press, 1963.

Allan, W. and Poulter, E. M.: ULF waves – their relationship to the structure of the Earth's magnetosphere, Rep. Prog. Phys., 55, 533–598, 1992.

Cross, R.: An introduction to Alfvén waves, IOP Publishing, Bristol, England, 1988.

Ellis, P. and Southwood, D. J.: Reflection of Alfvén waves by non-uniform ionospheres, Planet. Space Sci., 31, 107–117, 1983.

Hughes, W. J.: The effect of the atmosphere and ionosphere on long period magnetospheric micropulsations, Planet. Space Sci., 22, 1157–1172, 1974.

Hughes, W. J.: Hydromagnetic waves in the magnetosphere; In: Solar-terrestrial physics, edited by Carovillano, R. L. and Forbes, J. M., Reidel D. Pub. Co., Dordrecht, 453–477, 1983.

Hughes, W. J. and Southwood, D. J.: The screening of micropulsation signals by the atmosphere and ionosphere, J. Geophys. Res., 81, 3234–3240, 1976.

Miletits, J. Cz, Verö, J., Szendröi, J., Ivanova, P., Best, A. and Kivinen, M.: Pulsation periods at mid-latitudes – A seven-station study, Planet. Space Sci., 38, 85–95, 1990.

Miura, A., Ohtsuka, S., and Tamao, T.: Coupling instability of the shear Alfvén wave in the magnetosphere with ionospheric ion drift wave, 2. numerical analysis, J. Geophys. Res., 87, 843–851, 1982.

Nishida, A.: Ionospheric screening effect and storm sudden commencement, J. Geophys. Res., 69, 1861, 1964.

Nishida, A.: Geomagnetic diagnosis of the magnetosphere, Springer-Verlag, New York, 1978.

Ponomarenko, P. V., Waters, C. L., Sciffer, M. D., Fraser, B. J., and Samson, J. C.: Spatial structure of ULF waves: Comparison of magnetometer and super dual auroral radar network data, J. Geophys. Res., 106, 10 509–10 517, 2001.

Ponomarenko, P. V., Menk, F. W., and Waters, C. L.: Visualization of ULF waves in SuperDARN data, Geophys. Res. Lett., 30(18), 1926, doi:10.1029/2003GL017757, 2003.

Priest, E. R.: Solar magnetohydrodynamics, D. Reidel Pub. Co., Dordrecht, 1982.

Scholer, M.: On the motion of artifical ion clouds in the magnetosphere, Planet. Space Sci., 18, 977, 1970.

Sciffer, M. D. and Waters, C. L.: Propagation of mixed mode ULF waves through the ionosphere: Analytic solutions for oblique fields, J. Geophys. Res., 107, A10, 1297, doi:1029/2001JA000184, 2002.

Stix, T. H.: The theory of plasma waves, McGraw-Hill, New York, 1962.

Tamao, T.: The structure of three-dimensional hydromagnetic waves in a uniform cold plasma, J. Geomagn. Geoelectr., 16, 89–114, 1964.

Tamao, T.: Direct contribution of oblique field-aligned currents to the ground magnetic fields, J. Geophys. Res., 91, 183–189, 1986.

Waters, C. L., Menk, F. W., and Fraser, B. J.: The resonant structure of low latitude Pc 3 geomagnetic pulsations, Geophys. Res. Lett., 18, 2293–2296, 1991.

Waters, C. L., Sciffer, M. D., Fraser, B. J., Brand, K., Foulkes, K., Menk, F. W., Saka, O., and Yumoto, K.: The phase structure of very low latitude ULF waves across dawn, J. Geophys. Res., 106, 15 599–15 607, 2001.

Yoshikawa, A. and Itonaga, M.: Reflection of shear Alfvén waves at the ionosphere and the divergent Hall current, Geophys. Res. Lett., 23, 101–104, 1996.

Yoshikawa, A. and Itonaga, M.: The nature of reflection and mode conversion of MHD waves in the inductive ionosphere: Multistep mode conversion between divergent and rotational electric fields, J. Geophys. Res., 105, 10 565–10 584, 2000.

Yoshikawa, A., Obana, Y., Shinohara, M., Itonaga, M., and Yumoto, K.: Hall-induced inductive shielding effect on geomagnetic pulsations, Geophys. Res. Lett.,29(8), 10.1029/2001GL013610, 2002.

Ziesolleck C. W. S., Fraser, B. J., Menk, F. W., and McNabb, P. W.: Spatial characteristics of low-latitude Pc3–4 geomagnetic pulsations, J. Geophys. Res., 98, 197–207, 1993.

Zhang, D. Y. and Cole, K. D.: Formulation and computation of hydromagnetic wave penetration into the equatorial ionosphere and atmosphere, J. Atmos. Terr. Phys., 57, 813–819, 1995.